

Antimo Glorioso<sup>2</sup>, Francesco Petrosino<sup>1</sup>, Mattia Barbarino<sup>1</sup>, Giuseppe Pezzella<sup>2</sup> & Antonio Viviani<sup>2</sup>

<sup>1</sup>CIRA—Italian Aerospace Research Centre, Capua (CE), 81043, Italy <sup>2</sup>Università degli Studi della Campania "Luigi Vanvitelli", Aversa (CE), 81031, Italy

### **Abstract**

The design of a supersonic aircraft is directly connected with the signature pressure that results in a specific sonic boom noise. The focus of this work is to evaluate and compare the sonic boom of three different supersonic aircraft concepts through a numerical approach. A dedicated computational procedure was developed. First, aerodynamic near-field simulations are performed using the open-source solver SU2. The pressure signature at different locations on the vertical plane is evaluated, a focus at different positions around the aircraft is also carried out. A detailed comparison between the three different concepts was conducted in term of noise performances.

**Keywords:** Aeroacoustics; Noise; Sonic Boom; CFD, Propagation.

### 1. Introduction

Over the past two decades, there has been a renewed focus on developing a new generation of supersonic aircraft for civil use[1]. Research indicates that there is likely a viable market for such aircraft under certain economic conditions. Although numerous concepts are in development worldwide, none have yet entered operation, primarily due to environmental concerns such as noise pollution and higher emissions[2]. A major challenge in supersonic aircraft development is reducing the noise generated by the shock waves, commonly known as the sonic boom[3].

Currently, most countries prohibit supersonic flights over land due to the disturbance caused by sonic booms. However, the ability to fly at supersonic speeds over land is considered essential for the economic viability of these aircraft. Various technologies and techniques have been developed to better predict and mitigate sonic boom impacts, aiming to meet future regulatory limits[4]. Achieving these limits is particularly challenging for large aircraft due to their size and lift requirements. With the growing interest in sustainable supersonic aircraft, there is a surge in research on innovative designs that could meet future sustainability standards. Establishing an acceptable level of sonic boom annoyance is a crucial task for regulatory bodies to ensure that these aircraft can operate at supersonic speeds in the future[5].

Since 2014, NASA has supported the AIAA Sonic Boom Prediction Workshop[6][7][8], which aims to establish numerical methodologies for predicting sonic booms. The cross-validated methodologies and results from the workshop participants represent the current state-of-the-art in predicting sonic booms in the near-field region of an aircraft. The published methodologies and case studies from the workshop form the basis for the studies presented in this paper.

The simulation of sonic boom propagation is typically divided into two regions: the near-field domain and the far-field domain. The near-field domain encompasses the area close to the aircraft where shock formation occurs, characterized by strong non-linear phenomena such as shock-shock interactions, shock bending, and cross flow. This region is generally analyzed using Computational Fluid Dynamics (CFD) with various numerical techniques[9][10]. Consequently, the accuracy of sonic boom predictions is highly dependent on the precision of near-field simulations and signatures.

Operating conditions	Value	
Mach number	2.0	
Angle of attack [deg]	0	
Altitude [m]	15760	
Pressure [Pa]	10684.3	
Temperature [K]	216.6	

Table 1 – Simulation parameters

The numerical approach proposed in literature allows for the characterization of novel aircraft designs[11], like a Mach 5 waverider configuration[12]. The computed near-field pressure fields from this work facilitate far-field shock wave propagation computations for on-ground signature analyses and annoyance assessments of the sonic boom.

This paper further validate NASA's proposed hybrid numerical approach for the evaluation of sonic boom phenomenon of supersonic aircraft in terms of pressure signature computed in near-field for different aeroshapes, by using Computational Fluid Dynamics (CFD). The open source flow solver SU2 Multiphysics Simulation and Design Software[13] is considered for the flowfield simulations, using the numerical scheme HLLC[14] on hybrid computational mesh grid. Several numerical investigations are dedicated to evaluate the pressure signature of three different aeroshape concepts, to furthermore compare the noise performance of each aircraft.

The activities described in this paper are part of the H2020 MORE&LESS project (MDO and Regulations for Low Boom and Environmentally Sustainable Supersonic Aviation)[15]. This project, in response to the EC call "Towards global environmental regulation of supersonic aviation" (LC-MG-1-15-2020), aims to support Europe in shaping global environmental regulations for future supersonic aviation. Recommendations are based on the outcomes of extensive high-fidelity modeling activities and test campaigns, which are integrated into a multi-disciplinary optimization framework to assess the holistic impact of supersonic aviation on the environment.

The first part of this work focuses on the aerodynamic near-field domain, in particular the prediction of the pressure signature for three supersonic aircraft, identified with the names CS1a, CS2 and CS3, developed in the framework of the MORE&LESS project. A detailed overview of the geometries is given in sections 2.1 2.2 and 2.3 respectively. In the following section 3, an extensive comparison between the three aircraft is carried out, in term of geometries and sonic boom generation.

## 2. Geometries and Near Field Modelling

Open source code SU2[13] was chosen as computational tool to evaluate the aerodynamic near-field solutions. This solver uses an unstructured finite-volume approach to solve the Reynolds-Averaged Navier-Stokes (RANS) equations. The gradients are computed using a Green–Gauss approach. The CFL value was fixed to a unitary value in the convergence strategy. Simulations are executed solving inviscid Euler equations with ideal gas model for air phase, therefore no effect of physical viscosity was considered. Across several numerical schemes available, the HLLC[14] is selected, following the results of previous published works[9][10].

The computational mesh production follows the guideline highlighted in the above mentioned reference works. As exposed in Figure 1, the computational domain is decomposed in two zones: an inner part near the aircraft constructed with an unstructured approach, while the outer part far from the aircraft used a structured approach. In addition, the outer part is inclined following the angle of the Mach cone related to the particular operating condition.

The three aircraft of this work were investigated under the same operating conditions, reported in table 1. Using the same parameters was necessary to have a better comparison of noise performances.

The pressure signature in the aeroacoustic problems is typically evaluated using the formulation:

$$dp/p = \frac{p_s - p_0}{p_0} \tag{1}$$

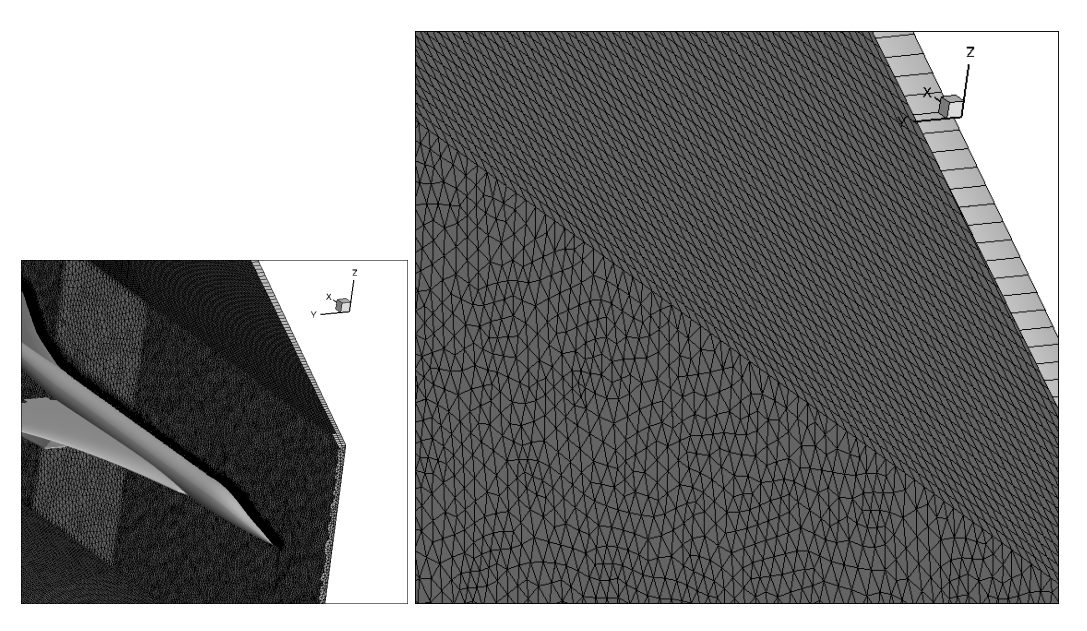


Figure 1 – CS1a computational hybrid mesh, particular of unstructured and structured zone.

In equation 1, the variable  $p_0$  is the free-stream static pressure, while  $p_s$  is the pressure variations extracted at a specific H/L location, where H is the vertical distance from the aircraft, and L is the length of the vehicle.

# 2.1 CS1a geometry

The first aircraft investigated is labeled CS1a, visible in Figure 2. This design of the aircraft was developed in the framework of the European project MORE&LESS.

This aircraft concept was derived from the Concorde aircraft, with the objective to improve its environmental impact. The main differences between the CS1a and the Concorde geometries are the dimension of the wings, without curvature, and engine nacelles shape. The body length is 62m and the wing area is  $166.3m^2$ .

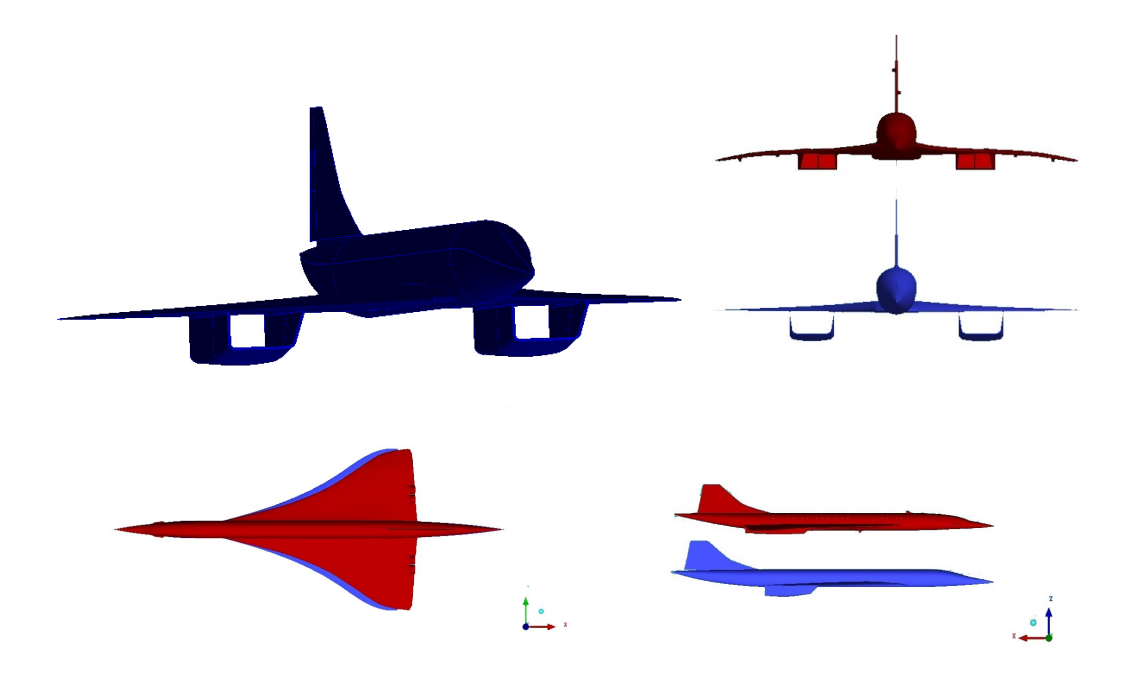


Figure 2 – CS1a geometry (blue), comparison with the Concorde aircraft (red).

The size of the computational mesh produced to solve the aerodynamic near-field was approximately 26.5 million elements.

Figure 3 shows the pressure signature extracted along an horizontal plane at distance from the aircraft  $(\frac{H}{L}) = 3$ . In this picture, the black vertical lines highlight the positions of the nose and the end of the aircraft, the blue vertical lines highlight the positions of the leading edge and the trailing edge of the wing.

Three overpressure peaks are visible, the first two are due to the compression of the fluid at the nose and the leading edge of the wing, while the last one is due to the expansion of the fluid, it is caused by the end of the wing.

Figure 4 shows the pressure signature at distances  $(\frac{H}{L}) = 1$  (left image) and  $(\frac{H}{L}) = 5$  (right image). Similar behaviour of pressure signature for  $(\frac{H}{L}) = 3$  is visible, the intensity of pressure peaks reflects the different distance from the body between each extraction position.

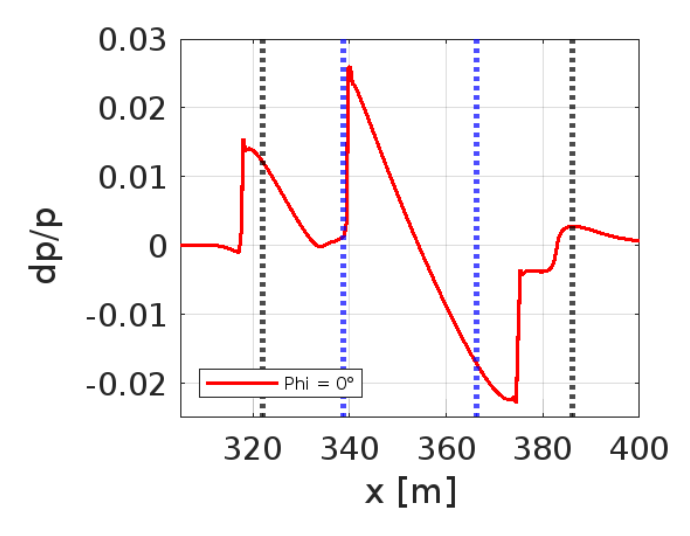


Figure 3 – CS1a pressure signature, distance from aircraft  $(\frac{H}{I})_3$ .

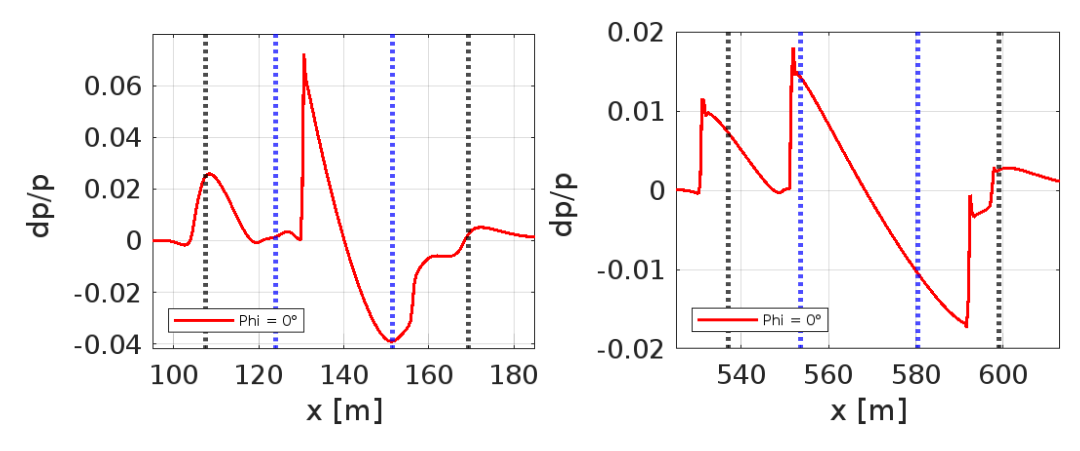


Figure 4 – CS1a pressure signature, distance  $(\frac{H}{L})_1$  (left) and  $(\frac{H}{L})_5$  (rigth).

Contours of Mach number and pressure field in terms of pressure variation  $\frac{dp}{p}$  are shown in Figure 5. Shock waves are well highlighted, consistently with the pressure signature results shown in the previous figures.

An investigation of the pressure signature variations around the aircraft was also carried out, as visible in Figure 6, where the radial angle  $\phi$  represents the position  $\phi = 0^{\circ}$  under the aircraft, up to  $\phi = 180^{\circ}$  above the aircraft. In the left part of Figure 6 the scheme of radial positions is reported, in the middle picture the pressure signatures for different radial position is reported, it is possible to highlight difference in pressure variation due to the complicated geometry analysed, with wing, engine nacelles, tail. In the right picture of Figure 6 we reported the highest value of pressure in decibels for each radial position, computed at the three reference distances from the aircraft. As already shown, there is no symmetry in noise values around the aircraft according to the geometry of the vehicle, it is possible also evaluate the reduction in noise values moving away from the CS1a,

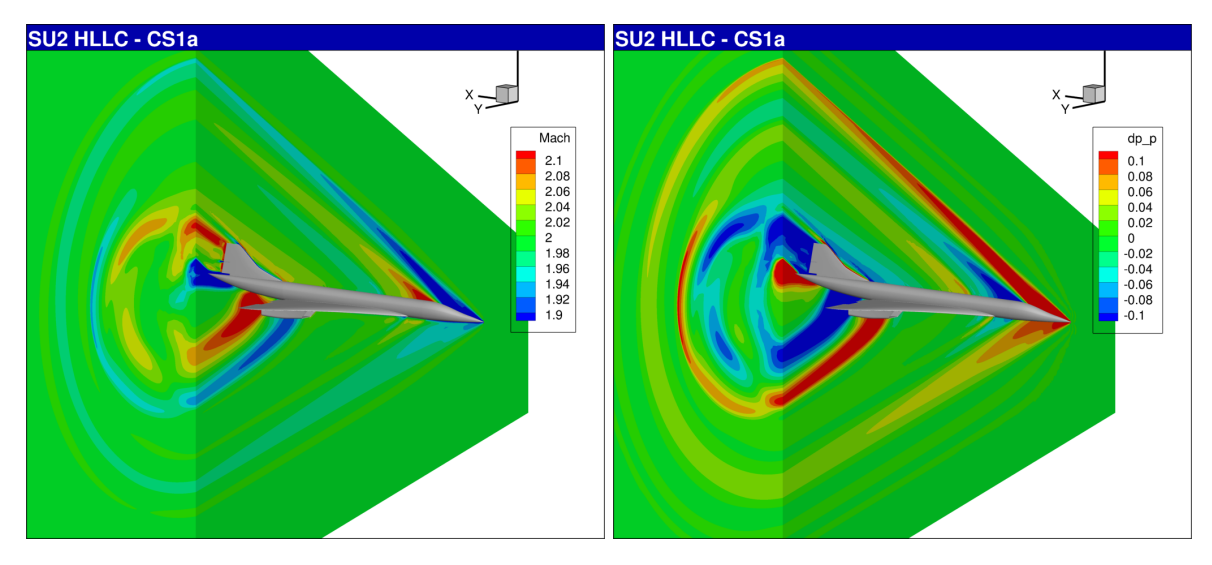


Figure 5 – CS1a contour of Mach number (left) and  $\frac{dp}{p}$  (right).

as expected from noise propagation theory.

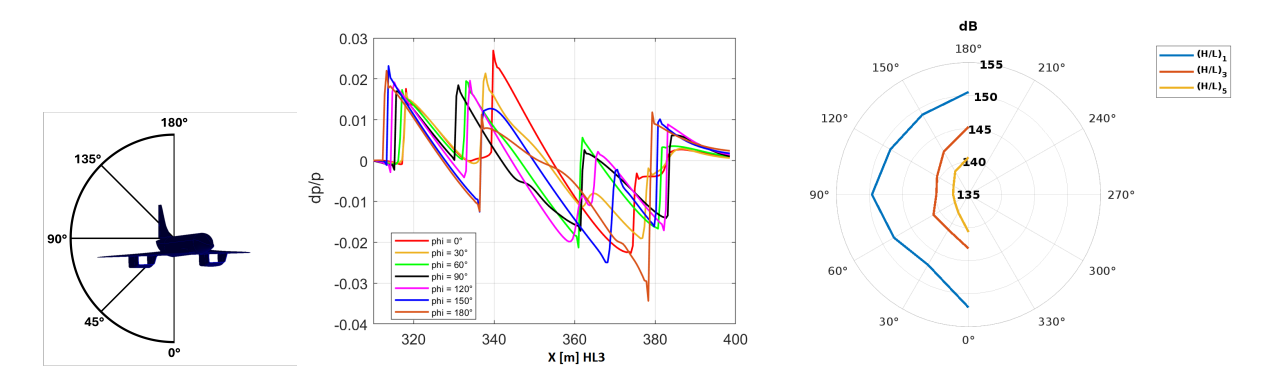


Figure 6 – CS1a noise: radial scheme (left), pressure signatures (center) and dB - highest peak (right).

## 2.2 CS2 geometry

The second aircraft investigated is labelled CS2, geometry is reported in Figure 7. This is the second vehicle developed in the framework of the European project MORE&LESS. The body length is 24.53m and the wing area is  $40.77m^2$ . The aircraft was developed by Reaction Engine, partner of the project, with the aim to produce a Hypersonic Test Bed to evaluate different engine concepts. In out work, we considered the aircraft without additional engines.

The size of the computational mesh produced to solve the aerodynamic near-field was approximately 11.6 million elements.

The flowfield simulation was at same operating condition of CS1a geometry, therefore similar analysis were carried out. Figure 8 shows the pressure signature computed under the aircraft at distance from the vehicle  $(\frac{H}{L}) = 3$ . As for the CS1a, in the figure are highlighted the begin and end of the aircraft with two vertical black lines, and the leading and trailing edge of the main wing. Three expansion peaks and two compression peaks are visible. The first peak is related to the nose and the canard wing, while the second peak is due to the leading edge of the main wing of the airplane. The last peak is correlated to the end of the aircraft and the stability of the fluid that return in the freestream conditions. Figure 9 shows the pressure signature at distance  $(\frac{H}{L}) = 1$  and  $(\frac{H}{L}) = 5$ , no difference behaviour compared to the position  $(\frac{H}{L}) = 3$ , the intensities of the peaks are different due to the different distances from the body of each extraction position.

different distances from the body of each extraction position. Contours of Mach number and  $\frac{dp}{p}$  are shown in Figure 10, the Mach waves and the expansion and compression zone are well defined, as expected from the pressure signature curves. The results of

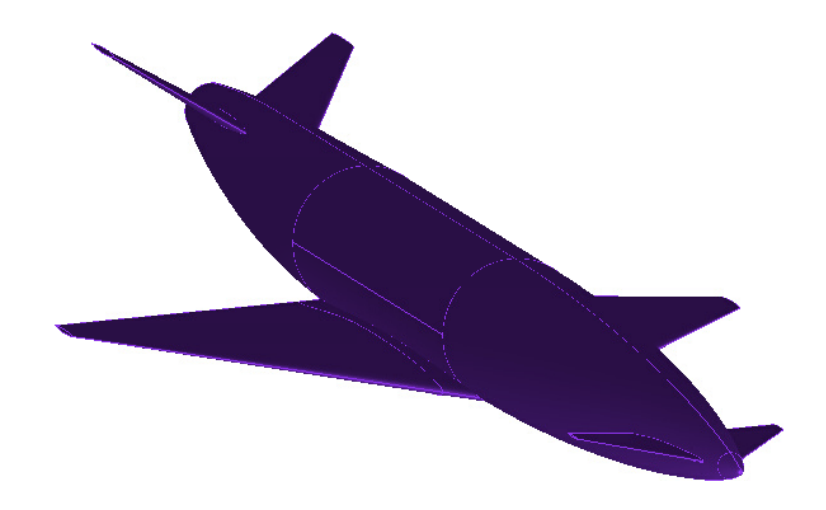


Figure 7 – CS2 geometry.

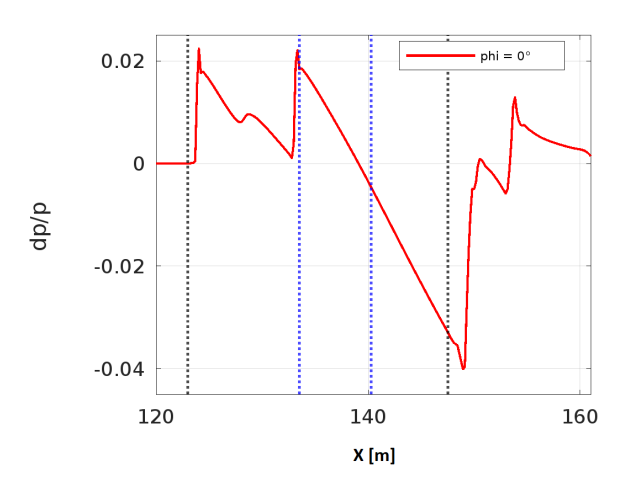


Figure 8 – CS2 pressure signature, distance from the aircraft  $(\frac{H}{I})_3$ .

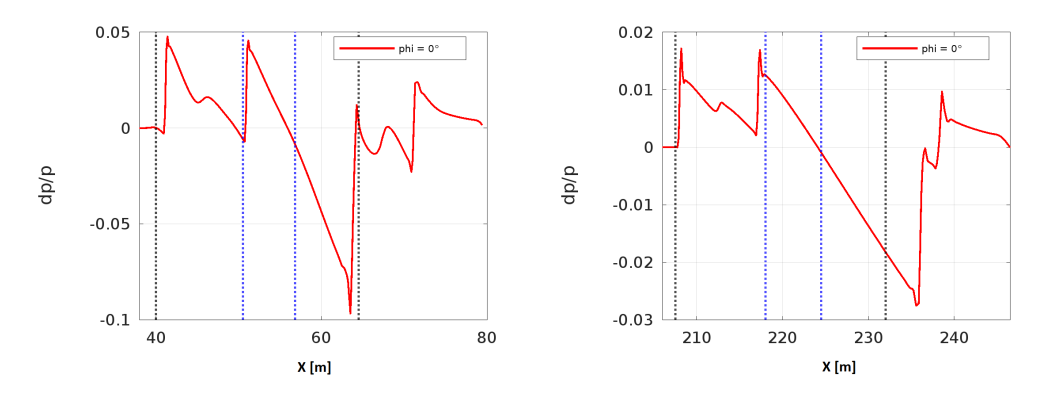


Figure 9 – CS2 pressure signature, distance  $(\frac{H}{L})_1$  (left) and  $(\frac{H}{L})_5$  (rigth).

CS2 geometry are very similar to CS1a outcomes, since the two geometries have similar geometric characteristics, like main wing, additional aerodynamic surfaces, a defined fuselage.

The variation of pressure signature values around the aircraft is carried out using the same approach of CS1a case. In Figure 11 from the angle  $\phi = 0^{\circ}$  that is the position under the aircraft, to the angle  $\phi = 180^{\circ}$  that is the position above the vehicle, pressure signature at distance  $(\frac{H}{L}) = 3$  were extracted and reported. In the zone under the CS2 geometry we found the greatest values of sonic boom, while in the other positions it is possible to notice the presence of aerodynamic interference that reduce

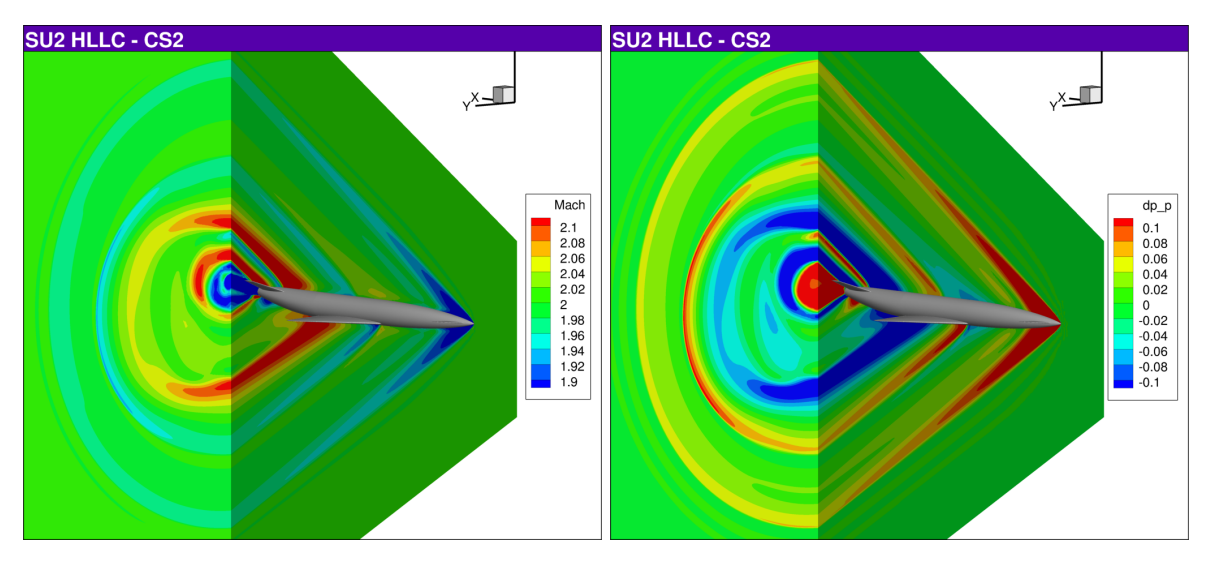


Figure 10 – CS2 contour Mach number (left) and contour  $\frac{dp}{p}$  (right)

and modify the pressure variations. In the right part of Figure 11 is shown the highest value of noise in decibels, for each radial positions analysed, and for the three reference distances considered. As for CS1a, there is no symmetry noise distribution around the aircraft, and the propagation of the sonic boom moving far from the vehicle shown a reduction of values as expected.

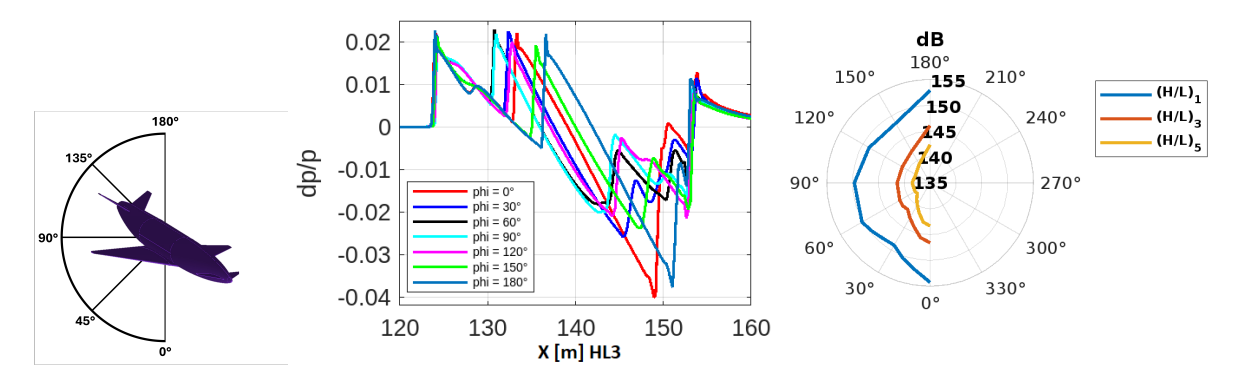


Figure 11 – CS2 noise: radial scheme (left), pressure signatures (center) and dB - highest peak (right).

## 2.3 CS3 geometry

The third aircraft investigated is labeled CS3, visible in Figure 12. This aircraft was derived from a Mach 8 vehicle developed in the STRATOFLY project[16], adapted to accomplish the performances requested in the MORE&LESS project. The body length is 75m and the wing area is  $1000m^2$ .

The size of the computational mesh produced to solve the aerodynamic near-field was approximately 13 million elements.

Also in this case, the operating condition are the same of previous geometries. Figure 13 shows the pressure signature evaluated for the CS3 on a horizontal plane at distance  $(\frac{H}{L}) = 3$  from the aircraft. Due to the particular design of the CS3 vehicle, it could be considered a full wing aircraft, in the picture we reported two black lines only that represents the begin and the end of the geometry. As a design consequence, the pressure signature of CS3 has the shape of classical N-wave. Some small peaks are visible near to the highest and lowest values of pressure variation, related to the canard wing in the front zone and the end of the vehicle in the rear part. Figure 14 shows the pressure signature at distance  $(\frac{H}{L}) = 1$  and  $(\frac{H}{L}) = 5$ . In the proximity of the aircraft, distance  $(\frac{H}{L}) = 1$ , the N-shape in visible but some difference is present due to the flow field that is not completely developed. At relevant distance from CS3, position of extraction  $(\frac{H}{L}) = 5$ , the dissipation of the shock waves tends to merge the small peaks in a single better defined N-wave.

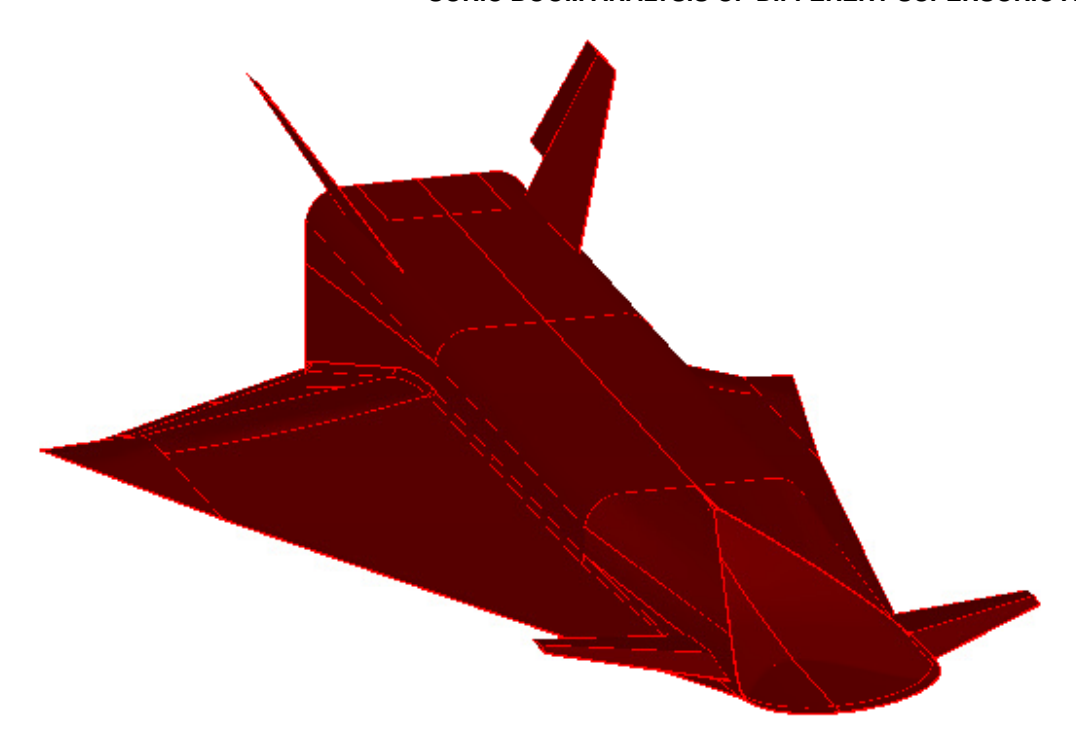


Figure 12 - CS3 geometry.

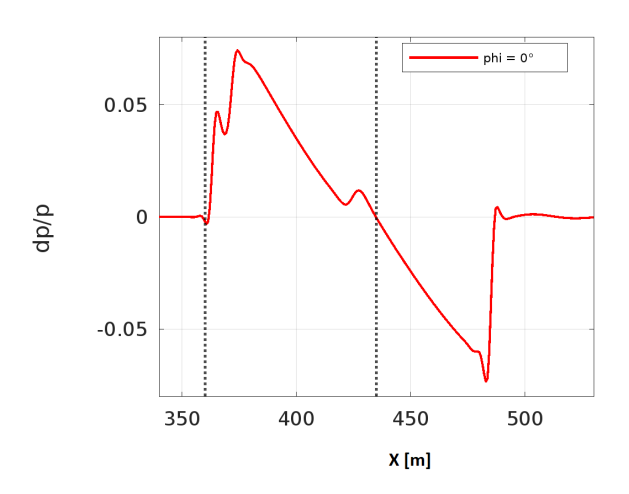


Figure 13 – CS3 pressure signature, distance from the aircraft  $(\frac{H}{L})_3$ .

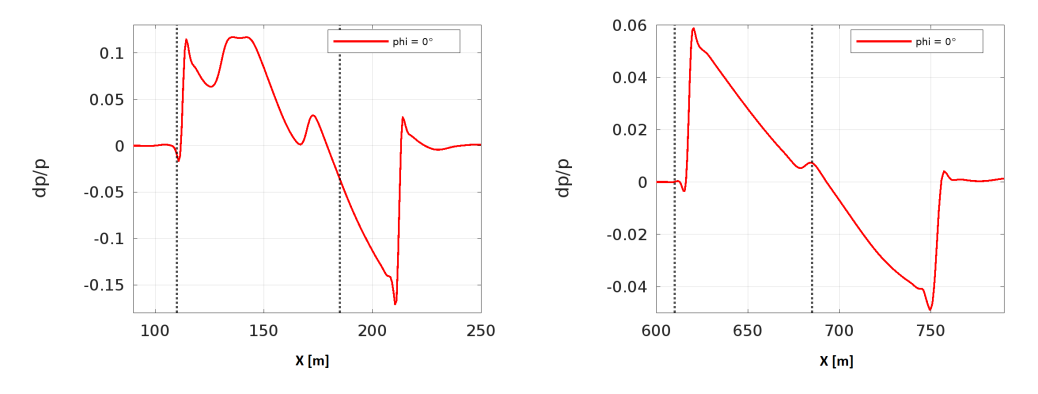


Figure 14 – CS3 pressure signature, distance  $(\frac{H}{L})_1$  (left) and  $(\frac{H}{L})_5$  (rigth).

The presence of single shock is highlighted in the contours of Mach number and  $\frac{dp}{p}$  of Figure 15. A

strong and well-defined zone is visible, without several small shock waves as previous cases.

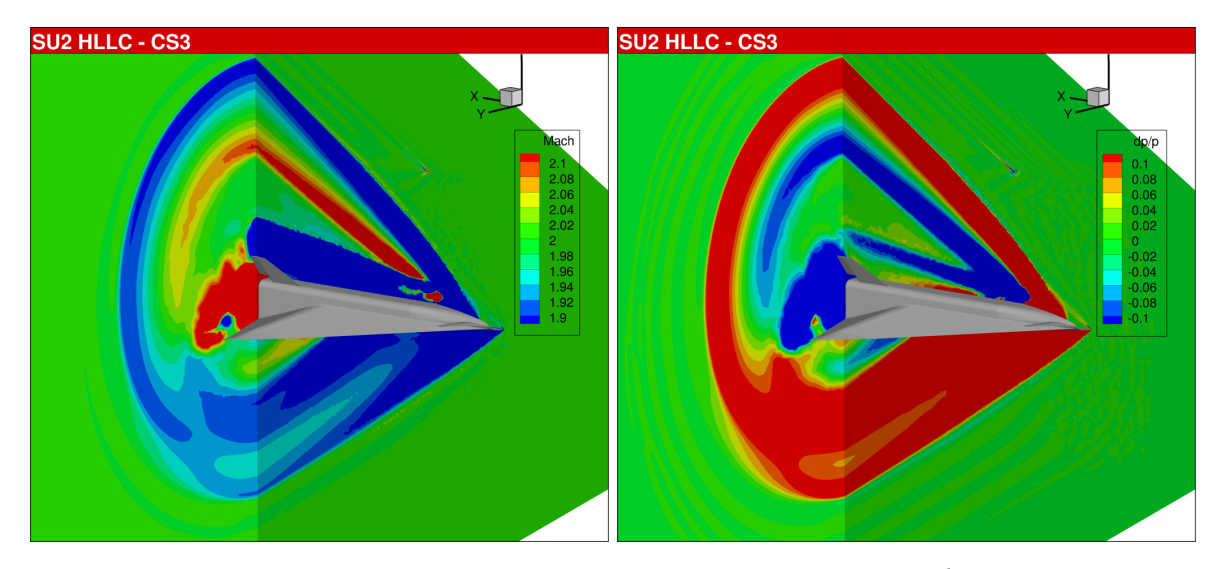


Figure 15 – CS3 contours Mach number (left) and contours  $\frac{dp}{p}$  (right).

The review of pressure signature variation in the radial positions around the CS3 geometry is reported in Figure 16. As for the previous considerations, the pressure signature under the vehicle for radial angle  $\phi = 0^{\circ}$  shows the maximum values compared to other positions, with effects of wing presence visible moving from under to upper part where  $\phi = 180^{\circ}$ . In the right picture of Figure 16 is shown the highest value of noise in decibels, for each radial positions analysed, and for the three reference distances considered. As for other cases, there is no symmetry noise distribution around the aircraft, and the propagation of the sonic boom moving far from the vehicle shown a reduction of values as expected.

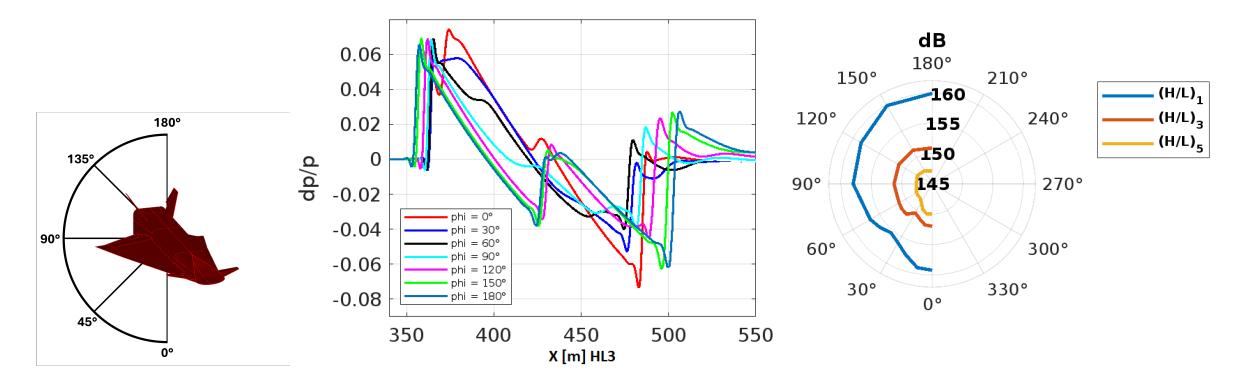


Figure 16 – CS3 noise: radial scheme (left), pressure signatures (center) and dB - highest peak (right).

# 3. Results of comparisons

In this paragraph, the work focuses on a comparison between the three aircraft concepts illustrated in the previous section.

A first geometrical comparison is carried out, the three geometries are superimposed in Figure 17, where black lines identify CS1a, red lines are for CS2, and purple lines draw the CS3 vehicle. The Figure 17 quickly shows the huge dimensions difference between the three geometries. A summary of the geometrical characteristics of the considered aircraft in reported in table 2. The CS1a has a traditional aircraft design, while the CS3 is a hypersonic concept aircraft with a wing-body and canard wing, the CS2 presents a hybrid shape between the classical aircraft and a more innovative design for supersonic flight. In addition, the CS2 is the shortest aircraft compared to CS1a and CS3, that have similar length.

Dimensions	CS1a	CS2	CS3
Body Length [m]	62	24.56	75
Body Height [m]	10	3.81	19.3
Wing Span [m]	26	8.67	40.5
$S_{ref} [m^2]$	166.3	40.77	1000

Table 2 – Aircraft dimensions comparison.

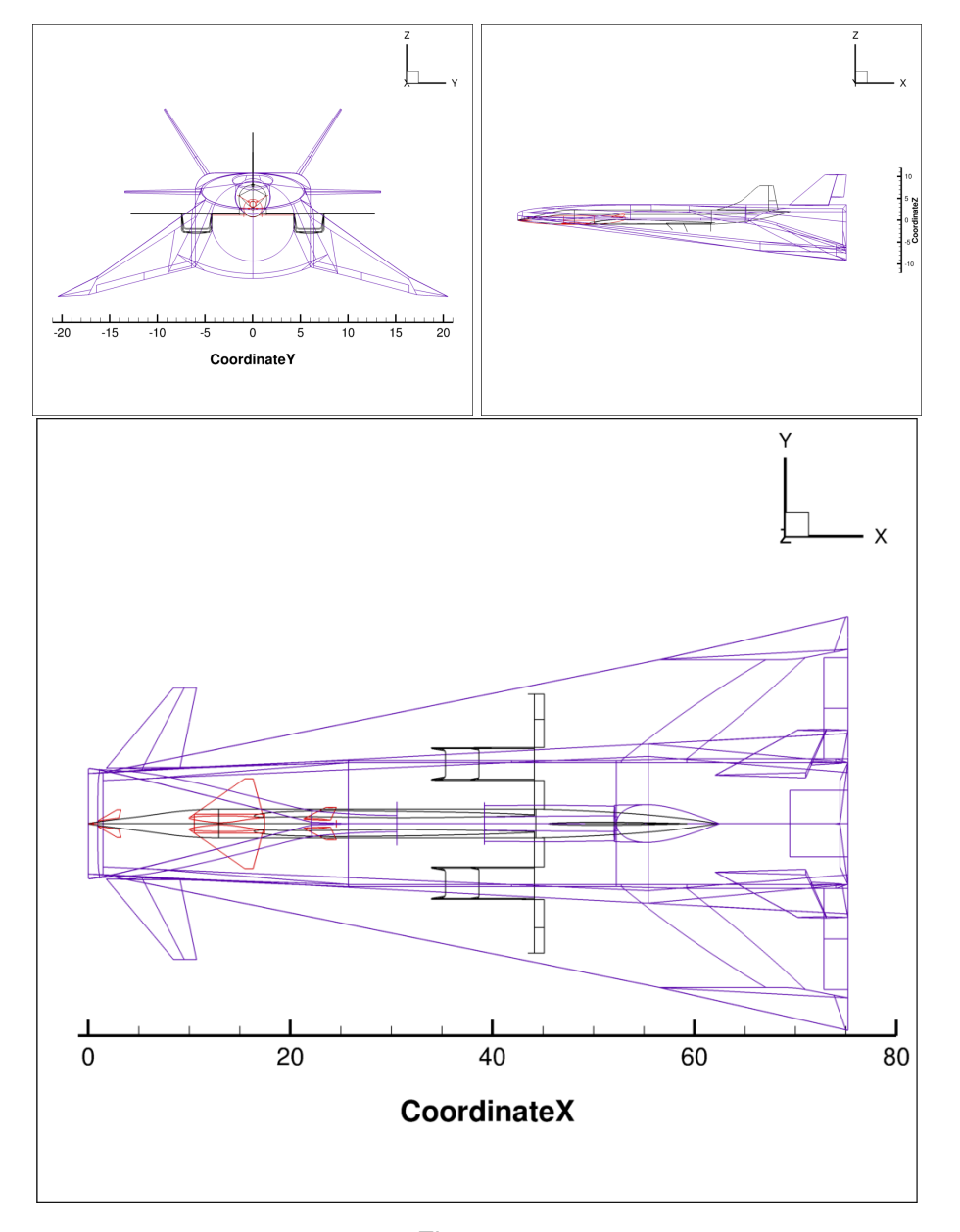


Figure 17

In the Figures from 18 to 20, the comparison between the pressure signature of each aircraft at reference distances  $(\frac{H}{L})_1$ ,  $(\frac{H}{L})_3$  and  $(\frac{H}{L})_5$  was carried out. In order to better compare pressure variations, the x-axis of those figures is a non-dimensional length, calculated dividing the dimensional length of the pressure results shown in the previous section, for the body length of each aircraft. This approach leads to similar pressure signature lengths, and highlight the differences of each aircraft design. CS1a and CS2 have a very similar pressure signatures, with a first pressure peak due to the shock waves near the nose of the aircraft, and a N-shape wave in the zone of the wings. The CS3 shows a bigger and longer signature compared to the other two vehicles, with several pressure peaks visible only in the zone close to the aircraft (distance  $\frac{H}{L} = 1$ ). Equivalent behaviour is visible in the right

pictures of Figures 18, 19 and 20, where the highest pressure values for each radial angle around the aircraft were reported in decibels. At each reference distance from the aircraft, CS1a and CS2 concepts have very close noise distribution, while the CS3 produces a noise field that is around 10dB greater than other two vehicles.

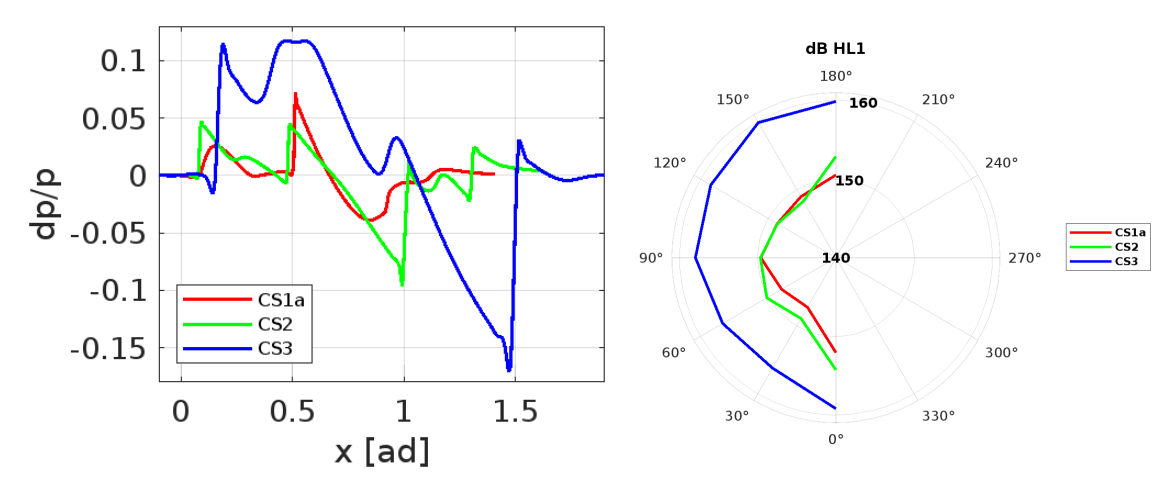


Figure 18 – Comparison of pressure signature at distance  $(\frac{H}{L})_1$  (left), noise distribution in decibel around the aircraft (right).

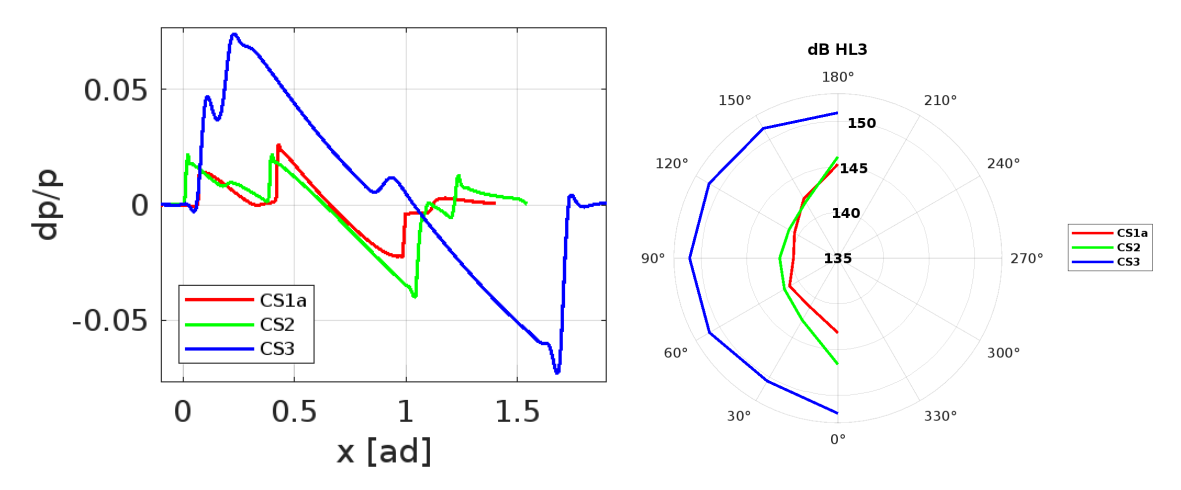


Figure 19 – Comparison of pressure signature at distance  $(\frac{H}{L})_3$  (left), noise distribution in decibel around the aircraft (right).

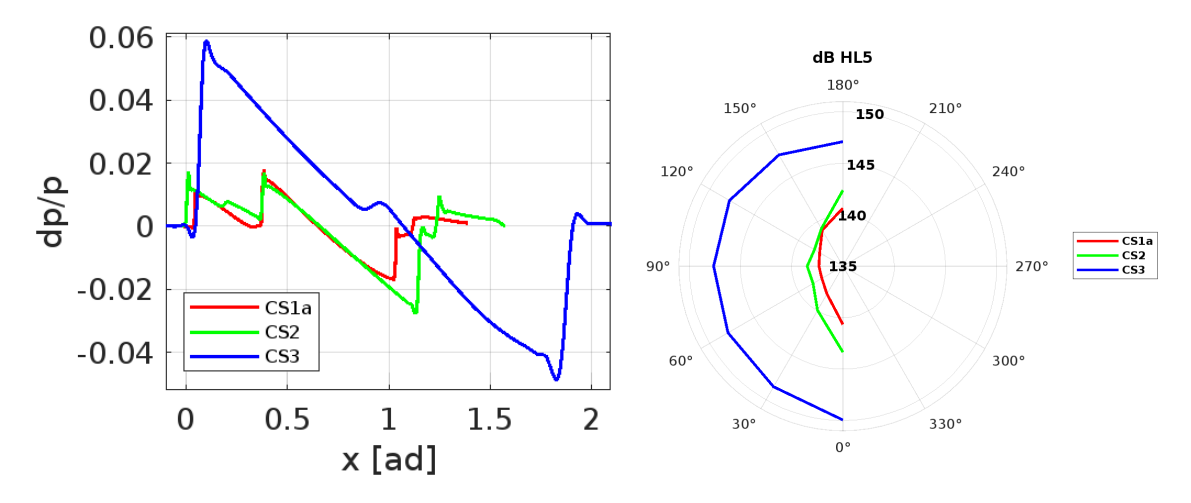


Figure 20 – Comparison of pressure signature at distance  $(\frac{H}{L})_5$  (left), noise distribution in decibel around the aircraft (right).

Those results highlight that the engineering design of the CS1a can be considered the best of the three aircraft in terms of noise performances, due to the noise field smaller than CS3 result and similar to the CS2 result, despite the huge difference in body length. This outcome was carried out at non-dimensional distance  $\frac{H}{L}$ . From the point of view of noise annoyance, we compared the sonic boom generated by each aircraft at the same physical distance, that can be identified as the solution at  $(\frac{H}{L})_1$  for CS1a and CS3, and at  $(\frac{H}{L})_3$  for CS2. The comparison is shown in Figure 21. At the same dimensional distance, the CS3 aircraft continue to produce the greatest values of noise, while the CS2 generates the lowest and shortest pressure signature. The CS1a results are in average position, in terms of pressure values and extension of signature. The values of the peaks pressure in decibels can be seen on the right part of Figure 21, where it is possible to highlight a difference of around 5dB between CS2 and CS1a, 10dB between CS1a and CS3. The CS2 makes the lowest sonic boom field, but the difference with the CS1a result is small, although the big difference in body length between them.

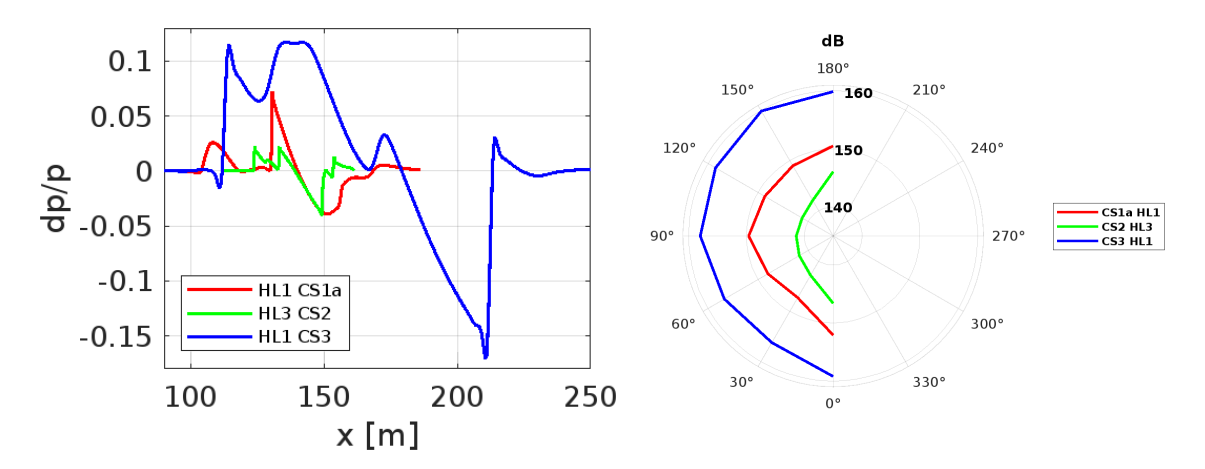


Figure 21 – Comparison of pressure signature at same dimensional distance (left), noise distribution in decibel around the aircraft (right).

Even if all the presented analyses were executed in the near field domain, an interesting effect of the sonic boom propagation is noticeable. Pressure signature of CS3 aircraft is plotted in Figure 22 for the three distances considered from the vehicle. Moving away from the body, the peaks of the pressure signature reduce and the curve stretches, as expected from the noise propagation physics. This effect is visible also for CS1a and CS2 geometries, comparing their pressure signatures of Figures 18, 19 and 20, but is more evident for CS3 aircraft. In addition, for the CS3 geometry, moving far from the aircraft, the pressure signature becomes a classic N-wave in near field domain, the peaks in the front zone merge into one peak, the same happen in the rear zone.

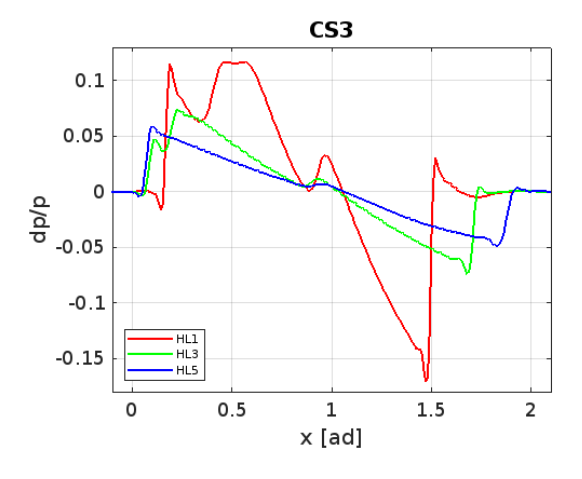


Figure 22 – Sonic boom propagation in near-field domain for CS3 aircraft.

The propagation of sonic boom in near field domain can be evaluated also in terms of maximum

values of pressure signature in decibels. For each case, Figures 23, 24 and 25 show the noise reduction moving away from the vehicles, computed in the plane under the aircraft that corresponds to angle  $\phi = 0^{\circ}$ , and in the radial planes related to angles  $\phi = 30^{\circ}$  and  $\phi = 60^{\circ}$ . In the position under the aircraft, the reduction of sonic boom noise is around 7dB between the distance  $(\frac{H}{L})_1$  and  $(\frac{H}{L})_3$ , and around 3dB between the distance  $(\frac{H}{L})_3$  and  $(\frac{H}{L})_5$ . In the other planes, the reduction is the same of position  $\phi = 0^{\circ}$ , but starting from lower values.

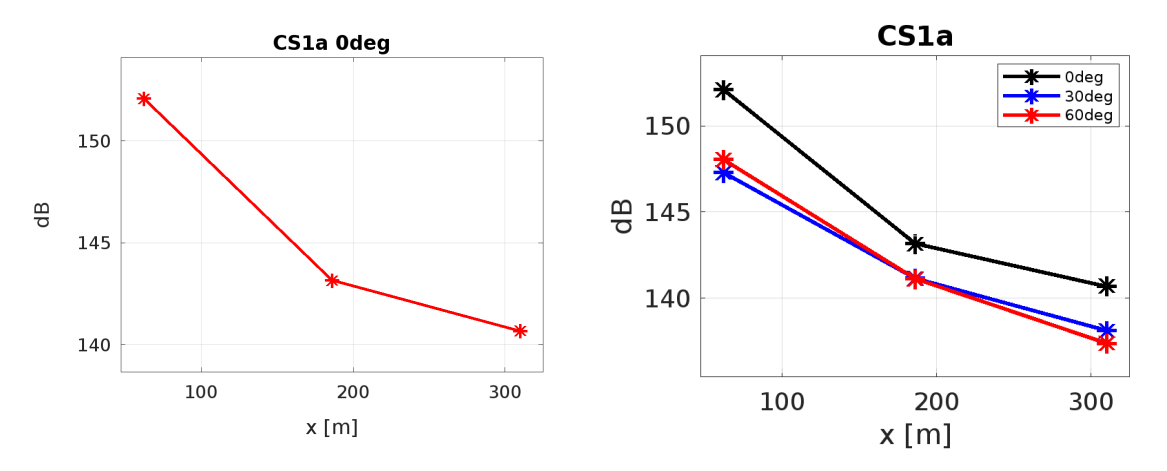


Figure 23 – CS1a, sonic boom propagation under the aircraft  $\phi = 0^{\circ}$  (left), and for different radial positions (right).

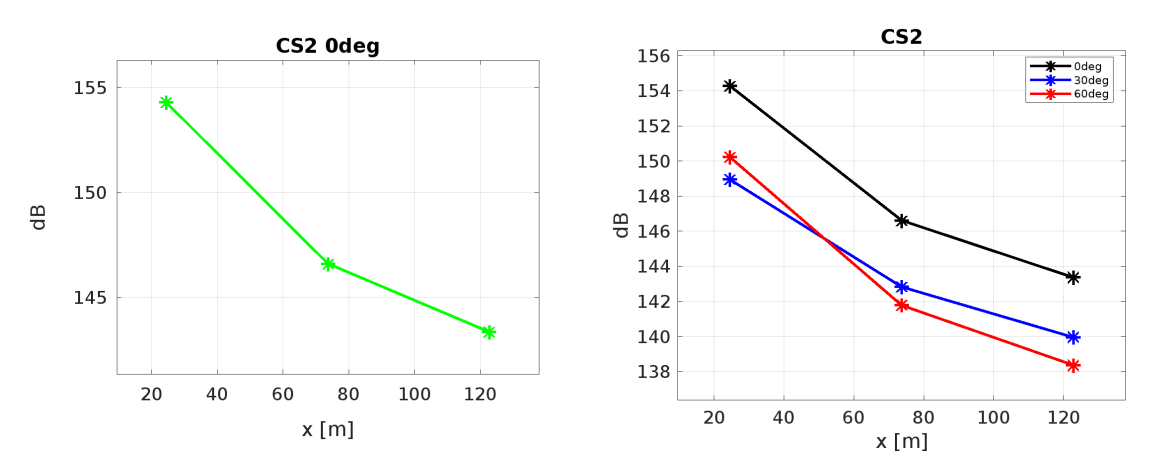


Figure 24 – CS2, sonic boom propagation under the aircraft  $\phi = 0^{\circ}$  (left), and for different radial positions (right).

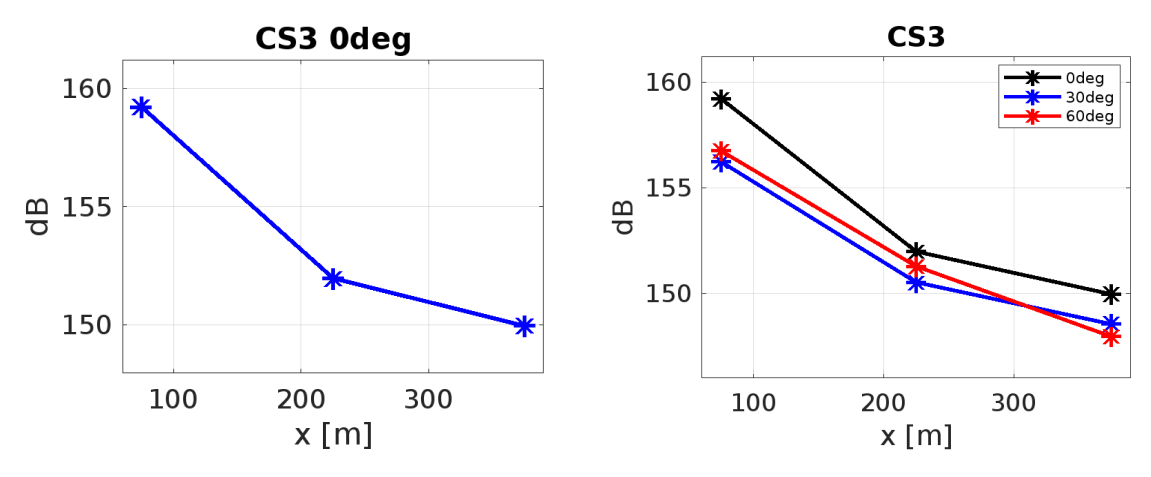


Figure 25 – CS3, sonic boom propagation under the aircraft  $\phi = 0^{\circ}$  (left), and for different radial positions (right).

### 4. Conclusions

Three aircraft concepts for supersonic flight were analysed in term of sonic boom generation in the near field zone.

The CS1a aircraft has a traditional aircraft shape, it was directly derived from the Concorde aircraft design. The CS2 concept is designed as a supersonic test bench for engines. The CS3 is a hypersonic concept aircraft with a wing-body and canard wing. For each test case, a computational mesh grid was produced, follow the literature best practices and previous experience, and the aerodynamic flowfield was simulated with the use of open-source solver SU2.

The pressure signature at different distances from the aircraft was evaluated, with particular focus on estimate the noise peak values around the geometry, in order to highlight the effects of wing and other aerodynamic surfaces.

An extensive comparison of noise performance was carried out. The similar shape of CS1a and CS2 aircraft leads to similar noise fields, while the CS3 produces the loudest sonic boom signature. The design of CS3 generates a pressure signature with a classical N-shape, due to the wing-body geometry. In the pressure field of CS1a and CS2 it is possible to notice the effect of shock waves generated by the nose of the vehicle with pressure values comparable to the shock waves generated by the wings. In absolute values, when compared at similar distance from the aircraft, the CS3 produces the highest noise levels, due to its shape and biggest dimensions when compared with the other geometries, while the CS2 has the lowest levels of noise, related to smallest body length. A final outcome is that the design of the CS1a is the best in terms of noise performances, with the lowest sonic boom generated compared to the results of CS2, that is noticeable smaller but produces similar levels of pressure variations, and to the results of CS3, that is dimensionally similar but produces a greater shock wave.

Analysing the pressure variation at different distance from the aircraft, the propagation of noise signature highlights the coalescence of pressure peaks in even more defined N-wave, while their values were reduced, as expected from the physics of the problem and confirming the soundness of the numerical approach adopted.

In conclusion, the numerical procedure applied to sonic boom evaluation of aircraft concepts shows good results to evaluate the noise performances of supersonic vehicle, in addition is able to estimate the effects of propagation of noise moving far from the generation zone.

#### 5. Contact Author Email Address

Mail to: f.petrosino@cira.it

## 6. Acknowledgments

The authors thank the MDO and Regulations for Low-boom and Environmentally Sustainable Supersonic aviation (MORE and LESS) project, that is a research project pursued by a consortium of

European government and academic institutions, including the Italian Aerospace Research Centre (CIRA) and coordinated by Politecnico di Torino under the EC Horizon 2020 financial support (Grant Agreement 101006856). MORE and LESS aims to address the challenges regarding the environmental impact of the supersonic, air-breathing aviation implementing a holistic approach based on a synergic coupling between low and high-fidelity modelling of several processes e.g., aerodynamics, jet-noise, sonic-boom, propulsion, and above all pollutant and climate-changing chemical emissions.

## 7. Copyright Statement

The authors confirm that they, and/or their company or organization, hold copyright on all of the original material included in this paper. The authors also confirm that they have obtained permission, from the copyright holder of any third party material included in this paper, to publish it as part of their paper. The authors confirm that they give permission, or have obtained permission from the copyright holder of this paper, for the publication and distribution of this paper as part of the ICAS proceedings or as individual off-prints from the proceedings.

### References

- [1] Liebhardt B., Lütjens K. An Analysis of the Market Environment for Supersonic Business Jets. *DLRK Tagungsband 2011: 60. Deutscher Luft- und Raumfahrtkongress in Bremen*, 2011, https://elib.dlr.de/75275/
- [2] Sun Y., Smith H. Review and prospect of supersonic business jet design. *Progress in Aerospace Sciences*, Vol. 90, pp 12-38, 2017, https://doi.org/10.1016/j.paerosci.2016.12.003
- [3] Marulo F. Aircraft Community Noise: The Revenge of a Neglected Problem. *Aerotecnica Missili & Spazio*, Vol. 94, pp 184-194, 2015, https://doi.org/10.1007/BF03404700
- [4] Maglieri D. J., Bobbitt P. J., Plotkin K. J., Shepherd K. P., Coen P. G., Richwine D. M. Sonic boom: Six decades of research. *NASA SP-2014-622*, 2014, https://ntrs.nasa.gov/citations/20150006843
- [5] Rötger T., Eyers C., Fusaro R. A Review of the Current Regulatory Framework for Supersonic Civil Aircraft: Noise and Emissions Regulations. *Aerospace*, Vol. 11, No. 1, 2024, https://doi.org/10.3390/aerospace11010019
- [6] Park M., Morgenstern J. Summary and Statistical Analysis of the First AIAA Sonic Boom Prediction Workshop, 32nd AIAA Applied Aerodynamics Conference, 16-20 June 2014 Atlanta, GA, https://doi.org/10.2514/6.2014-2006
- [7] Park M. A., Nemec M. Nearfield Summary and Statistical Analysis of the Second AIAA Sonic Boom Prediction Workshop. *Journal of Aircraft*, Vol. 56, No. 3, pp 851-875, 2019, https://doi.org/10.2514/1.C034866
- [8] Park M. A., Carter M. B. Nearfield Summary and Analysis of the Third AIAA Sonic Boom Prediction Workshop C608 Low Boom Demonstrator. AIAA Scitech 2021 Forum, 11-15 January 2021, Virtual Event, https://doi.org/10.2514/6.2021-0345
- [9] Glorioso A., Petrosino F., Aprovitola A., Barbarino M., Pezzella G. Sonic Boom generation using open source CFD approach. *AIAA AVIATION 2023 Forum*, 12-16 June 2023 San Diego, CA, https://doi.org/10.2514/6.2023-4168
- [10] Glorioso A., Petrosino F., Barbarino M., Pezzella G., Viviani A. Improvement on Open Source CFD Methodology To Evaluate Near-Field Sonic Boom. 30th AIAA/CEAS Aeroacoustics Conference, 4-7 June 2024, Rome, Italy, https://doi.org/10.2514/6.2024-3185
- [11] Roncioni P. Marini M., Gori O., Fusaro R., Viola N. Aerodatabase Development and Integration and Mission Analysis of a Mach 2 Supersonic Civil Aircraft. *Aerospace*, Vol. 11, No. 2, 2024, https://doi.org/10.3390/aerospace11020111
- [12] Viola N., Roncioni P., Gori O., Fusaro R. Aerodynamic Characterization of Hypersonic Transportation Systems and Its Impact on Mission Analysis. *Energies*, Vol. 14, No. 12, 2021, https://doi.org/10.3390/en14123580
- [13] Economon T. D. et ali. SU2: An Open-Source Suite for Multiphysics Simulation and Design. *AIAA Journal*, American Institute of Aeronautics and Astronautics, 2016, https://doi.org/10.2514/1.J053813
- [14] Toro E.F., Spruce M. Restoration of the contact surface in the HLL-Riemann solver. *Shock Waves*, Vol. 4, No. 4, pp 25-34, 1994, https://doi.org/10.1007/BF01414629
- [15] Horizon 2020. MDO and REgulations for Low-boom and Environmentally Sustainable Supersonic aviation. *Grant agreement ID:* 101006856, 2021, https://doi.org/10.3030/101006856
- [16] Viola N., Fusaro R., Gori O., Marini M., Roncioni P., Saccone G., Saracoglu B., Ispir A. C., Fureby C., Nilson T., Iron C., Vincent A., Martinez Schramm J., Grewe V., Emmerig J., Hauglustaine D., Linke F.,

Bodmer D. STRATOFLY MR3 – how to reduce the environmental impact of high-speed transportation. *AIAA Scitech 2021 Forum*, 11-15 January 2021, Virtual Event, https://doi.org/10.2514/6.2021-1877